


SCIENTIFIC REPORTS



OPEN

Effects of disorder induced by heavy-ion irradiation on $(\text{Ba}_{1-x}\text{K}_x)\text{Fe}_2\text{As}_2$ single crystals, within the three-band Eliashberg s_{\pm} wave model

G. Ghigo^{1,2}, G. A. Ummarino^{1,3}, L. Gozzelino^{1,2}, R. Gerbaldo^{1,2}, F. Laviano^{1,2}, D. Torsello^{1,2}  & T. Tamegai⁴

One of the open issues concerning iron-based superconductors is whether the s_{\pm} wave model is able to account for the overall effects of impurity scattering, including the low rate of decrease of the critical temperature with the impurity concentration. Here we investigate $\text{Ba}_{1-x}\text{K}_x\text{Fe}_2\text{As}_2$ crystals where disorder is introduced by Au-ion irradiation. Critical temperature, T_c and London penetration depth, λ_L , were measured by a microwave resonator technique, for different values of the irradiation fluence. We compared experimental data with calculations made on the basis of the three-band Eliashberg equations, suitably accounting for the impurity scattering. We show that this approach is able to explain in a consistent way the effects of disorder both on T_c and on $\lambda_L(T)$, within the s_{\pm} wave model. In particular, a change of curvature in the low-temperature $\lambda_L(T)$ curves for the most irradiated crystals is fairly well reproduced.

The s_{\pm} phase^{1,2}, an extended s-wave pairing with a sign reversal of the order parameter between different Fermi surface sheets, is the leading candidate for describing the pairing state in most of the iron based superconductors (IBS), including the BaFe_2As_2 family. According to this approach, superconductivity in these compounds is unconventional and mediated by antiferromagnetic spin fluctuations. However, a general consensus has not been achieved yet, also because of a number of experiments on the effects of non-magnetic impurities that apparently do not fit the s_{\pm} scenario. In particular, several substitution and particle-irradiation studies reported a much weaker rate of suppression of the critical temperature as a function of the scattering rate than initially suggested for a sign-changing order parameter^{3,4}. Moreover, other unconventional mechanisms have been put forth for describing IBS, e.g. the orbital fluctuations, which favors the s_{++} state without sign reversal⁵. A disorder-induced change from sign-reversed (s_{\pm}) to sign-preserved (s_{++}) symmetry in multi-band superconductors has been predicted^{6,7} and observed⁸. Finally, nodal-like behaviors at increasing disorder was observed, e.g. in highly substituted crystals⁹. Nevertheless, these evidences are not necessarily against the s_{\pm} picture in disordered samples. As a matter of fact, numerous unexpected novel superconducting properties, including non-trivial impurity effects – that can be even mistaken as evidence for a nodal gap state – can be explained within the s_{\pm} wave model. This was demonstrated by two-gap analyses^{10,11}, but should be quantitatively confirmed by a comparison of experimental results to more complete models, capturing the rich and complex physics of the material. In fact, there is evidence that at least three bands are required to satisfactorily describe the physical properties of BaFeAs -based compounds¹².

In this work, we study the effects of disorder on $\text{Ba}_{1-x}\text{K}_x\text{Fe}_2\text{As}_2$ crystals, with the aim to determine if a discrepancy exists between the disorder-induced suppression of T_c and the modifications of the London penetration

¹Politecnico di Torino, Department of Applied Science and Technology, Torino, 10129, Italy. ²Istituto Nazionale di Fisica Nucleare, Sez. Torino, Torino, 10125, Italy. ³National Research Nuclear University MEPhI (Moscow Engineering Physics Institute), Moskva, 115409, Russia. ⁴The University of Tokyo, Department of Applied Physics, Hongo, Bunkyo-ku, Tokyo, 113-8656, Japan. Correspondence and requests for materials should be addressed to G.G. (email: gianluca.ghigo@polito.it)

depth (λ_L) on one hand, and the theoretical expectation for the $s\pm$ phase on the other hand. Indeed, the analysis of $\lambda_L(T)$ and its modifications as a function of the rate of scattering by impurities has been used to shed light on the order parameter symmetry, the presence of nodes, and whether they are accidental or symmetry-imposed. A standard scheme proposed in literature is the following¹³: in the case of a superconductor with line nodes, impurity scattering is expected to change the linear temperature dependence of the penetration depth at $T \ll T_c$ to become quadratic. On the other hand, intraband scattering would lift the c -axis line nodes in the case of an extended s -wave and induce a change from T^2 to an exponential behavior¹⁴. On the contrary, if the starting system is a fully-gapped superconductor, introducing pair-breaking scattering would result in a change from exponential to T^2 variation, and to lower power in the presence of accidental nodes¹¹.

We tested this scheme with samples where disorder was introduced by 250-MeV Au-ion irradiation. Particle irradiation is the way to induce defects without contributing extra charge or huge structural distortions, contrary to most cases of chemical substitutions. Several experiments have been performed with iron-based superconductors in the last years^{10,15–28}, but due to the large variety of used particles and compounds, a clear picture has not been reached yet, and a systematic study is still lacking. TEM microscopy revealed that 200-MeV Au-ion irradiation of $\text{Ba}_{1-x}\text{K}_x\text{Fe}_2\text{As}_2$ crystals results in the formation of defects that are linearly correlated along the ion track but – contrary to the case of high- T_c cuprates – due to the metallic nature of the compound, they are discontinuous (30–240 nm in length)²⁷. In fact, magneto-optical imaging showed the clear signature of anisotropic flux pinning by discontinuous tracks in crystals irradiated with Au ions at the higher energy of 2 GeV²⁰, which are present also with irradiation at lower energies (250 MeV)²⁹. Moreover, a significant difference with respect to cuprates emerged from a STM analysis of irradiated Fe(Se,Te) crystals, showing that columnar defects produced by 250-MeV Au-ions have a metallic core²⁸, instead of the insulating core of the amorphous tracks that the same ions with the same energy produce in cuprates³⁰. In addition, significant defects other than correlated tracks are produced, such as smaller and more distributed cascades, beside the effects of secondary electrons and strain.

In fact, our data on heavy-ion irradiated $\text{Ba}_{1-x}\text{K}_x\text{Fe}_2\text{As}_2$ crystals do not seem to fit any case of the simplified $\lambda_L(T)$ scheme described above. Thus, a more general theoretical approach is needed to describe the experimental results. Two main aspects in this regard are to be considered: the multi-band nature of the system and the effect of disorder. On one hand, Eliashberg's theory is the optimal model to describe these systems. Within this approach and especially when the number of bands is higher than two, disorder can be conveniently treated within the Born approximation³¹, otherwise the T-matrix calculation would increase the number of parameters, making the comparison with experimental data more questionable and possibly not conclusive. Within the Born approximation, the model is sensitive to the global effect of disorder rather than to the details of defects. As a matter of fact, a more general theory to study the role of defects in superconductors was developed^{32–34}, but in the proposed formulation only applies to two-band systems, even if its generalization to more bands is possible. Since there is evidence that in the system under study the inter-band coupling is predominant and the number of bands to be considered is greater than or equal to three^{35,36}, and since using two-band models would lead to the appearance of intra-band terms that do not have a physical interpretation³⁷, we preferred to consider three conducting bands, rather than a more precise parametrization of disorder. Being convinced that this approach is decisive for capturing the essential physics of the material, even if other aspects are unavoidably disregarded, we considered a three-band Eliashberg model, simple enough to allow a meaningful comparison with experimental results. Within this frame, the comparison led us to the awareness that the $s\pm$ wave model is able to reconcile apparently different evidences, once the impurity scattering role is accounted for.

Techniques

High-quality $\text{Ba}_{1-x}\text{K}_x\text{Fe}_2\text{As}_2$ crystals with an analyzed doping level of $x = 0.42$ were grown by the FeAs self-flux method²⁶, and cut as thin plates with thickness (along the c -axis) of about 10 μm , much smaller than width and length. Disorder was induced by 250-MeV Au-ion irradiation, with the ion beam parallel to the c -axis of the crystals.

The characterization of the crystals is carried out by a microwave superconducting resonator technique, in a cavity perturbation approach^{38,39}, described in the *Methods* section, allowing us to determine the critical temperature and the penetration depth of small crystals.

Experimental data are discussed within the $s\pm$ wave model in the presence of impurity scattering, by comparing them to calculations based on the solution of the three-band Eliashberg equations with suitable input conditions, as detailed below.

Results

Suppression and broadening of the superconducting transition. A first characterization of the superconducting transition and its modification after irradiation – in terms of temperature and width – can be obtained from rough data, without any model or analysis assumption. The inset in Fig. 1 shows the temperature dependence of the inverse of the unloaded quality factor when the $\text{Ba}_{1-x}\text{K}_x\text{Fe}_2\text{As}_2$ crystal is coupled to the resonator, normalized to its value at $T = 40$ K (see the *Methods* section for details). Since $1/Q_0$ is proportional to losses, such curves are qualitatively comparable to surface resistance curves. Data are shown for the same crystal before and after subsequent irradiations, up to the fluence of $3.6 \times 10^{12} \text{ cm}^{-2}$. In the mainframe, derivatives are reported, clearly showing that irradiations cause T_c suppression and broadening of the transition. More meaningful values of T_c , useful for a quantitative comparison with theoretical calculations, will be obtained below after the determination of the penetration depth.

Effects of irradiation on the penetration depth. Figure 2 shows the London penetration depth λ_L as a function of temperature, for the same crystal before and after subsequent irradiations. The effect of ion irradiation is both to enhance the λ_L values and to modify its temperature dependence. First of all, we investigate the

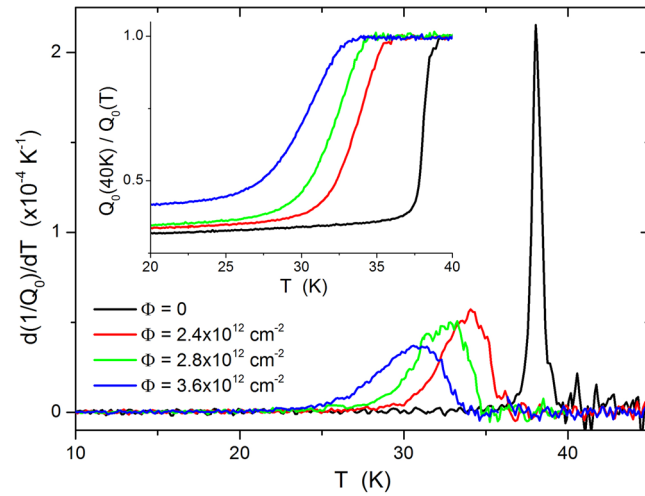


Figure 1. Temperature and width of the superconducting transition, from rough data. The inset shows the temperature dependence of the inverse of the resonator quality factor in the presence of the $\text{Ba}_{1-x}\text{K}_x\text{Fe}_2\text{As}_2$ sample, normalized to its value at $T = 40$ K. Data are shown for the same crystal before and after subsequent irradiations. In the mainframe, derivatives are reported, showing that irradiations cause T_c suppression and transition-width enlargement.

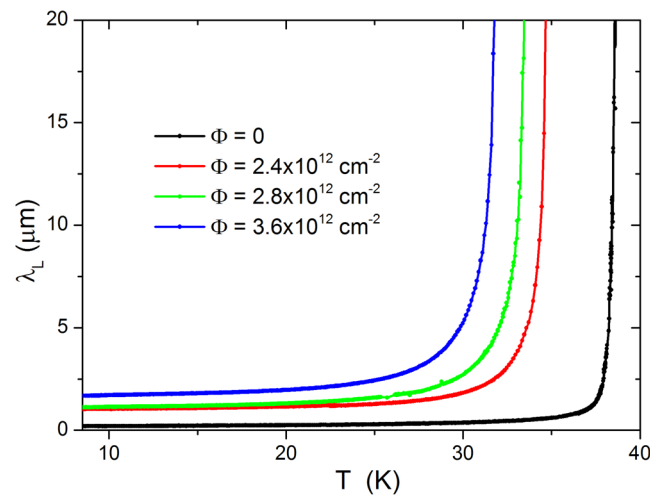


Figure 2. Penetration depth as a function of temperature, for the same $\text{Ba}_{1-x}\text{K}_x\text{Fe}_2\text{As}_2$ crystal, before and after subsequent irradiations up to a total fluence of $\Phi = 3.6 \times 10^{12} \text{ cm}^{-2}$.

low-temperature behavior of λ_L in order to check if it can be understood within the standard scheme described in the Introduction. Data below $T/T_c = 0.35$ are fitted to a power law, $\Delta\lambda_L \propto T^n$. Figure 3 reports the exponent n for unirradiated and irradiated samples, as a function of the fluence. Dashed lines indicate reference literature values: an exponent n higher than 3 can be considered to approach the exponential behavior, which is indicative of a fully-gapped clean s -wave state. On the other side, a d -wave state would imply $n \approx 1$. In both the cases, the addition of impurity-driven scattering would lead to the dirty limit at $n \approx 2$. This is not the trend we observed (symbols), since a smooth decrease from $n \gg 3$ to $n < 1$ is clearly shown, as the irradiation fluence is increased. It must be noted that the temperature evolution shown in Fig. 3 is not strictly speaking the low-temperature asymptotic one, that is not accessible by the experiment. Nevertheless, it gives the qualitative indication that a more rigorous theoretical approach is needed to describe the experimental data.

Three-band Eliashberg s_{\pm} calculations. To understand these results, a comparison with a theoretical model capturing the essential physics of the material is needed. We used a three-band Eliashberg s_{\pm} wave model in the presence of impurity scattering, with the constraint that both the T_c suppression and the $\lambda_L(T)$ behavior were simultaneously explained. The electronic structure of the compound $\text{Ba}_{1-x}\text{K}_x\text{Fe}_2\text{As}_2$ can be approximately described by two hole bands α, β (indicated in the following as bands 1 and 2) and one equivalent electron band γ (indicated in the following as band 3)⁴⁰. Within the s_{\pm} wave model, coupling between the electron and the hole

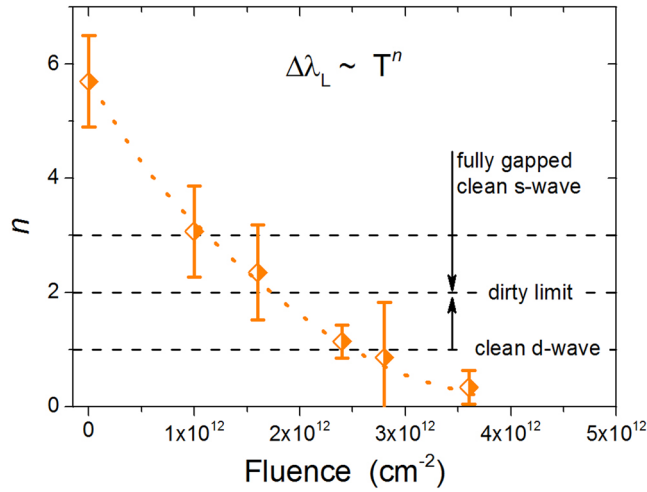


Figure 3. Exponent n of the $\lambda_L(T)$ power law for unirradiated and irradiated samples, as a function of the fluence. For the determination of n , an upper limit for the temperature range of $T/T_c = 0.35$ was adopted. Dashed lines set reference values (see text), while the dotted line is a guide for the eye.

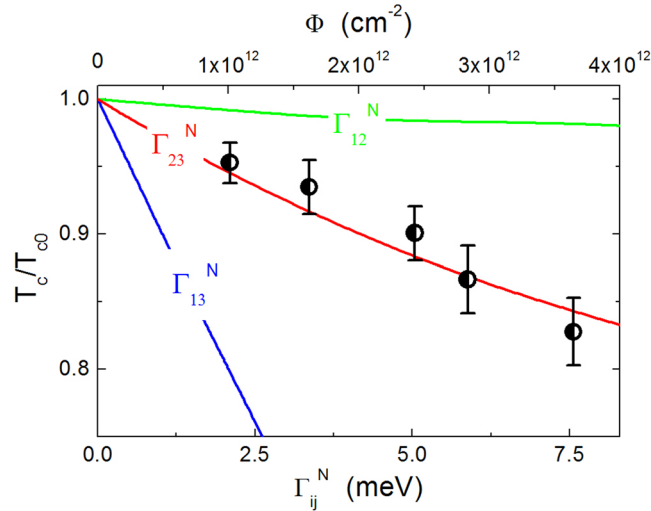


Figure 4. Critical temperature of the irradiated samples, T_c , normalized by the critical temperature of the unirradiated sample, T_{c0} , as a function of the interband scattering rate, Γ_{ij}^N (lower scale). The lines represent the three possible interband scattering channels, between bands 1, 2 and 3. Experimental data (symbols) are reported as a function of the fluence (upper scale). The upper and lower abscissa have been scaled until data collapsed onto one of the theoretical curves (the scaling factor is $4.8 \times 10^{14} \text{ eV}^{-1} \text{ cm}^{-2}$; Γ_{23}^N was chosen for the reasons described in the text).

bands is due to the antiferromagnetic spin fluctuations, and the gap of the electron band, Δ_3 , has opposite sign with respect to the gaps of the hole bands, Δ_1 and Δ_2 ¹. To calculate the gaps and the critical temperature by the three-band Eliashberg equations^{41–43} one has to solve six coupled equations for the gaps $\Delta_i(i\omega_n)$ and the renormalization functions $Z_i(i\omega_n)$, where i is a band index ranging from 1 to 3 and ω_n are the Matsubara frequencies (more details in the *Methods* section). The gaps are assumed to be isotropic due to the low values of anisotropy typical of optimally doped $\text{Ba}_{1-x}\text{K}_x\text{Fe}_2\text{As}_2$ (see also the discussion below). Moreover, considering gap anisotropy would complicate greatly the equations without significantly changing the physics of this system. The calculation is based on the assumption that the nonmagnetic impurity-scattering rates Γ_{ij}^N are directly proportional to the defect density that in turn is proportional to the irradiation fluence, while Γ_{ij}^N is taken to be zero for the unirradiated crystal. In principle, this introduces a lot of new free parameters (the Γ_{ij}^N constants are proportional to the structural disorder in an unknown way). Nevertheless, since the diagonal components Γ_{ii}^N do not affect the superconducting properties, we study separately the effects of pair-breaking Γ_{12}^N , Γ_{13}^N , and Γ_{23}^N .

For the sake of simplicity, we assume that disorder mainly affects only one of the interband channels. The lines in Fig. 4 represent the solutions of the Eliashberg equations for T_c/T_{c0} with disorder in the channels 12, 13, and 23,

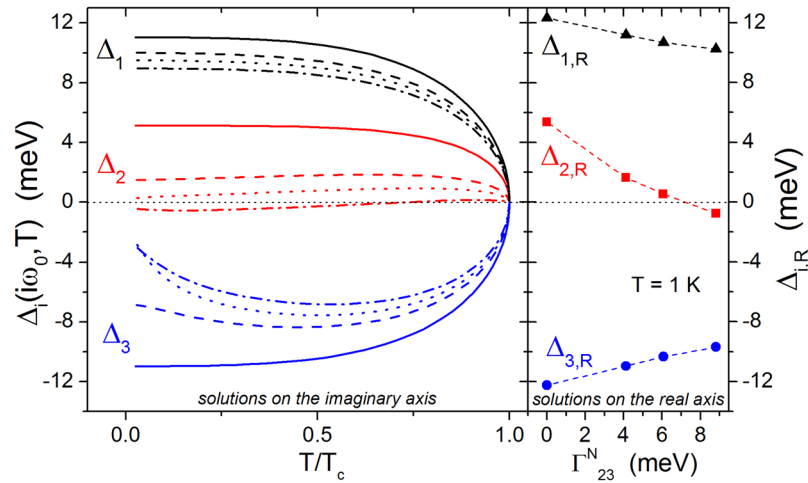


Figure 5. Left: temperature dependence of the first value of the energy gaps obtained by the solution of the imaginary-axis Eliashberg equations, Δ_1 (black), Δ_2 (red) and Δ_3 (blue) for the unirradiated material (solid lines) and for the material with the same level of disorder as the samples irradiated at the fluences Φ shown in Fig. 2, i.e. $\Phi = 2.4 \times 10^{12} \text{ cm}^{-2}$ ($\Gamma_{23}^N = 4.12 \text{ meV}$, dashed lines), $\Phi = 2.8 \times 10^{12} \text{ cm}^{-2}$ ($\Gamma_{23}^N = 6.07 \text{ meV}$, dotted lines), and $\Phi = 3.6 \times 10^{12} \text{ cm}^{-2}$ ($\Gamma_{23}^N = 8.81 \text{ meV}$, dashed dotted lines). Right: low-temperature values of the gaps from the real-axis solutions of the Eliashberg equations, obtained both by the Padé approximants and by a direct calculation, as a function of the scattering rate (dashed lines are guides to the eye).

respectively, as a function of the scattering rate (lower scale). The experimental data (symbols) are shown as a function of the irradiation fluence (upper scale). The two scales have been adjusted to obtain a good agreement between experimental data and the Γ_{23}^N curve, giving the scale factor between the fluence and the scattering rate ($4.8 \times 10^{14} \text{ eV}^{-1} \text{ cm}^{-2}$, in this case). Here the T_c value is determined as the temperature where $\lambda_L(T)$ diverges. Attempts to do the same with the Γ_{12}^N and Γ_{13}^N curves were not successful, i.e. did not lead to proper $\lambda_L(T)$ curves. We conclude here that the main mechanism responsible for T_c suppression is radiation-induced increase of the interband scattering rate between bands 2 and 3. Now the energy gaps can be calculated also for the irradiated crystals.

In Fig. 5 we report the gaps corresponding to the levels of disorder of the same sample as in Fig. 2, for each irradiation fluence (different colors for the three gaps and different line styles for the different fluences). The left-side panel shows the gap amplitudes obtained by the imaginary-axis solution of the Eliashberg equations. Remarkably, $\Delta_2(T)$ for the highest fluence changes sign. The right panel of Fig. 5 shows the real-axis low-temperature gap amplitudes, as a function of the interband scattering in the 23 channel. These values, deduced both by the Padé approximants and by a direct calculation on the real axis, are slightly different from the solutions on the imaginary axis, as expected because of the strong coupling regime. For the unirradiated-crystal case, we find gap values that are in fairly good agreement with earlier literature data⁴⁰. It is confirmed that the low-temperature Δ_2 value for the most disordered case is negative, both on the real and on the imaginary axis. It is also shown in Fig. 5 that Δ_2 for the most disordered case changes sign as a function of temperature. The change of sign as a function of scattering and/or temperature is worthy to be discussed in more detail.

A change of sign as a consequence of increased disorder was discussed in refs^{32–34}. To qualitatively understand this behavior in our case, it is sufficient to write the Eliashberg equation for the gap Δ_2 : $\Delta_2(i\omega_n)Z_2(i\omega_n) = \sum_m [-\lambda_{23}(i\omega_n - i\omega_m, T) + \Gamma_{23}^N \delta_{mn}] \Delta_3(i\omega_m, T) / \sqrt{\Delta_3^2(i\omega_m, T) + \omega_m^2}$, where λ_{23} , Γ_{23}^N and Z_2 are positive, while Δ_2 is negative and δ_{mn} is the Kronecker delta. The presence of disorder brings to an effective coupling (the quantity in the square bracket) that can change sign, resulting in a change of sign also for Δ_2 .

A sign change as a function of temperature was discussed in ref.⁴⁴. To understanding this particular effect it is sufficient to consider the previous equation for $n = 0$: $\Delta_2(i\omega_0)Z_2(i\omega_0) = \sum_m [-\lambda_{23}(i\omega_0 - i\omega_m, T) \Delta_3(i\omega_m, T) / \sqrt{\Delta_3^2(i\omega_m, T) + \omega_m^2} + \Gamma_{23}^N \Delta_3(i\omega_0, T) / \sqrt{\Delta_3^2(i\omega_0, T) + \omega_0^2}]$. When the temperature increases, the value of $\Delta_3(i\omega_0, T)$ decreases in absolute value. It can happen that the positive first term overcomes the negative second term, resulting in a change from negative to positive sign for Δ_2 .

Once the gaps and the main model parameters are calculated on the bases of the T_c behavior, the penetration depth can be computed by

$$\lambda^{-2}(T) = \left(\frac{\omega_p}{c}\right)^2 \sum_{i=1}^3 \left(\frac{\omega_{p,i}}{\omega_p}\right)^2 \pi T \sum_{n=-\infty}^{+\infty} \frac{\Delta_i^2(\omega_n) Z_i^2(\omega_n)}{[\omega_n^2 Z_i^2(\omega_n) + \Delta_i^2(\omega_n) Z_i^2(\omega_n)]^{3/2}} \quad (1)$$

where $\omega_{p,i}$ are the plasma frequencies of the three bands and ω_p is the total plasma frequency. Now, we can only act on the weights of the three bands, $\left(\frac{\omega_{p,i}}{\omega_p}\right)^2$ in order to adapt the calculation to the experimental $\lambda_L(T)$. The best results are reported in Fig. 6, where experimental $\Delta \lambda_L(T)$ (symbols) are compared to the calculations (lines).

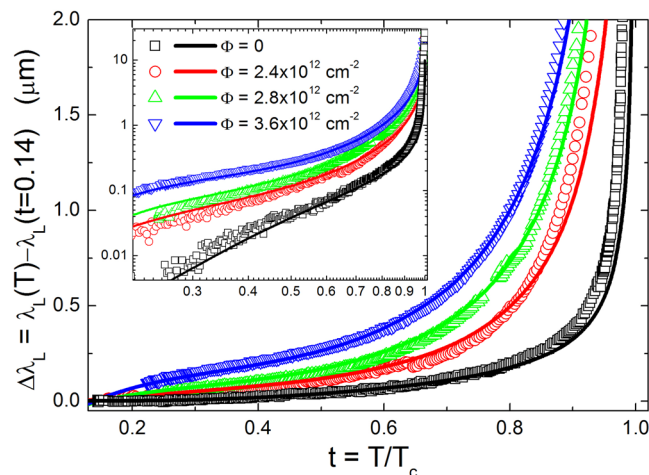


Figure 6. Penetration depth shift $\Delta\lambda_L(t) = \lambda_L(t) - \lambda_L(t=0.14)$, where $t = T/T_c$ is the reduced temperature. Experimental data (symbols) are compared to model calculations (lines), for the unirradiated sample ($\Phi = 0$) and for the same sample after subsequent irradiations, up to a total fluence $\Phi = 3.6 \times 10^{12} \text{ cm}^{-2}$. The inset shows the same data in a logarithmic scale.

Discussion and Conclusions

Iron-based superconductors display physical properties which are intimately related to their multiband structure. Since a subtle dependence of these properties on tiny impurity concentrations is expected, the investigation of the role of disorder in such compounds is crucial to achieve a comprehensive understanding. As stated in the Introduction, one of the issue still under debate is the symmetry of the superconducting order parameter, in spite of the huge efforts to conceile experiments with theoretical models. In fact, most of the analysis were done within a simplified two-band model, which is sometimes misleading. Here we have shown that a three-band approach is able to explain in a consistent way the effects of disorder both on T_c and on $\lambda_L(T)$, within the s_{\pm} wave model. Figure 6 shows a remarkable agreement between experiment and theory, in particular the change of curvature in the $\Delta\lambda_L(T)$ curves for the most irradiated cases is nicely reproduced.

Of course, the calculation still contains approximations and simplifications that could be refined. It is important to resume them and to estimate their possible influence to results. For example, we have found that the irradiation-induced scattering mainly affects the 23 interband channel: the selection of the 23 channel as the most significant follows the analysis of all the channels one by one, that is reasonable in view of a simplicity criterion. However, it cannot be excluded that other more complex combinations of the parameters could describe the experimental results as well, since it is reasonable that also the other channels are somehow modified. Moreover, we did not take into account the finite dimensions of the defects, and the presence of different kinds of defects (as stated in the Introduction, here disorder is treated in the Born approximation). The λ_L anisotropy was disregarded (in fact, it is among the lowest for iron-pnictides). Also the gap-anisotropy effect was not considered here. For example, we estimate that, if the smallest gap in k space was much smaller than the smallest average gap on one of the bands, the effect would be a decrease of the two free coupling constants (λ_{23} decreases in a more pronounced manner), but the critical temperature would not be affected significantly, since in this case it strongly depends on λ_{13} . Moreover, this material has already been studied – with good results – with an isotropic model⁴⁵ and the presence of disorder and the strong coupling regime reduce the impact of gap anisotropy⁴⁶. Finally, due to the proximity to a magnetic state in such compounds, the possibility of also inducing magnetic scattering by defects cannot be ruled out.

However, from the point of view of computation it is very hard to suitably consider all these aspects, and the adopted model is a good compromise between the need of a reliable tool to explain experimental trends and the need of physical correctness. In this sense, the best agreement between experiment and model shown in Fig. 6 led us to the following conclusions, some of them quantitative and some other only qualitative: (i) for the unirradiated sample, the weights of the three bands 1, 2 and 3 are 0.1, 0.8 and 0.1, respectively³⁸, and the total plasma frequency is $\omega_p = 1 \text{ eV}$, in nice agreement with ref.⁴⁷; (ii) the weight of the band 1 is not significantly affected by irradiation, while the weight of the band 2 decreases as a function of fluence and the weight of the band 3 increases; (iii) the total plasma frequency decreases as a function of fluence, down to the value of $\omega_p = 0.14 \text{ eV}$ for the most irradiated sample, in agreement with the observed increase of λ_L in irradiated samples; (iv) also a sub-linear λ_L temperature dependence is fully consistent with the s_{\pm} wave model, if the effects of impurity scattering is suitably taken into account.

Methods

Ion irradiation. Irradiations were performed at room temperature at the Tandem-XTU facility of the LNL laboratories of the Italian National Institute for Nuclear Physics (INFN). The ion beam was parallel to the c -axis of the crystals, and to minimize the heating of the crystals under irradiation, the ion flux was kept below $1.8 \times 10^8 \text{ cm}^{-2} \text{ s}^{-1}$. The highest fluence here considered is $3.6 \times 10^{12} \text{ cm}^{-2}$, corresponding to a dose-equivalent field of 72 T. The thickness of all the investigated samples is lower than the longitudinal range of the ions into the

material, that is about $14.5 \mu\text{m}$, as obtained by SRIM⁴⁸ and PHITS⁴⁹ code simulations, using the Kinchin-Pease approach. This guarantees that defects are introduced into the material without contributing extra charge. The overall damage can be computed by the mentioned codes, in terms of d.p.a. (displacements per atom, due to the elastic coulombian scattering against target nuclei), and of the total energy released by ionization. For the present experiment, we obtained the mean d.p.a. value of $7.6 \times 10^{-16} \times \Phi$, and a total energy release by ionization of $2.1 \times 10^{11} \times \Phi \text{ eV cm}^{-3}$, if the fluence Φ is expressed in cm^{-2} .

Measurements. In order to determine the critical temperature and the penetration depth we used a microwave resonator technique, in a cavity perturbation approach^{38,39}. The resonator is made of a $\text{YBa}_2\text{Cu}_3\text{O}_{7-x}$ film on MgO substrate, patterned in a coplanar geometry, with a $350\text{-}\mu\text{m}$ -wide central stripline⁵⁰. The $\text{Ba}_{1-x}\text{K}_x\text{Fe}_2\text{As}_2$ crystal is positioned by a small amount of high-vacuum grease in the center of the stripline, far from edges, i.e. in a region where the rf fields are uniform within about 5%. Measurements of the resonance curve are repeated in the same conditions, with and without the crystal, by means of a Rohde Schwarz ZVK vector network analyzer for an input power of -40 dBm , well below the non-linearity threshold for the resonator. The measurements were carried out in a Cryomech PT 415 pulse tube cooler.

The perturbations relative to no sample coupled to the resonator (rf field parallel to the broad face of the crystal), in terms of resonance frequency f_0 and quality factor Q_0 shifts, are⁵¹:

$$\frac{\Delta f_0}{f_0} = \frac{1}{2} \frac{V_s}{V_r} \left\{ 1 - \Re_c \left[\frac{\tanh(kc)}{kc} \right] \right\} \quad (2)$$

$$\Delta \left(\frac{1}{Q_0} \right) = \frac{V_s}{V_r} \Im_m \left[\frac{\tanh(kc)}{kc} \right] \quad (3)$$

where k is the complex propagation constant and c is the crystal half thickness. Here V_s is the volume of the sample and V_r is the effective volume of the resonator. The geometrical factor (V_s/V_r) is determined in a self-consistent way from data above T_c , where the crystals show a metallic behavior. In this case, $\Re_c(k) = \Im_m(k) = 1/\delta$ is imposed, where $\delta = \sqrt{2/\omega\mu\sigma}$ is the classical skin depth. Though most of the field penetrates through the broad faces of the crystals, suitable corrections are applied to account for the field penetration also along the sample thickness, due to the finiteness of the crystals (further details in the Supplementary Information). Once the geometrical factor is obtained, Eqs 2 and 3 allow obtaining the real and imaginary parts of the propagation constant k in the superconducting state, and in turn the London penetration depth λ_L and the normal conductivity σ_n , that are related to k by⁵²:

$$k = \left(\frac{1}{\lambda_L^2} + i\omega\mu_0\sigma_n \right)^{\frac{1}{2}}.$$

The model. As mentioned above, we considered a three-band Eliashberg $s \pm$ wave model in the presence of impurity scattering, by solving six coupled equations for the gaps $\Delta_i(i\omega_n)$ and the renormalization functions $Z_i(i\omega_n)$, where i is a band index ranging from 1 to 3 and ω_n are the Matsubara frequencies.

The imaginary-axis equations^{53–55} read:

$$\omega_n Z_i(i\omega_n) = \omega_n + \pi T \sum_{m,j} \Lambda_{ij}^Z(i\omega_n, i\omega_m) N_j^Z(i\omega_m) + \sum_j [\Gamma_{ij}^N + \Gamma_{ij}^M] N_j^Z(i\omega_n) \quad (4)$$

$$\begin{aligned} Z_i(i\omega_n) \Delta_i(i\omega_n) &= \pi T \sum_{m,j} \left[\Lambda_{ij}^\Delta(i\omega_n, i\omega_m) - \mu_{ij}^*(\omega_c) \right] \Theta(\omega_c - |\omega_m|) N_j^\Delta(i\omega_m) \\ &+ \sum_j [\Gamma_{ij}^N - \Gamma_{ij}^M] N_j^\Delta(i\omega_n) \end{aligned} \quad (5)$$

where Γ_{ij}^N and Γ_{ij}^M are the scattering rates from non-magnetic and magnetic impurities, respectively, $\Lambda_{ij}^Z(i\omega_n, i\omega_m) = \Lambda_{ij}^{ph}(i\omega_n, i\omega_m) + \Lambda_{ij}^{sf}(i\omega_n, i\omega_m)$ and $\Lambda_{ij}^\Delta(i\omega_n, i\omega_m) = \Lambda_{ij}^{ph}(i\omega_n, i\omega_m) - \Lambda_{ij}^{sf}(i\omega_n, i\omega_m)$ where

$$\Lambda_{ij}^{ph, sf}(i\omega_n, i\omega_m) = 2 \int_0^{+\infty} d\Omega \Omega \alpha_{ij}^2 F^{ph, sf}(\Omega) / [(\omega_n - \omega_m)^2 + \Omega^2].$$

Θ is the Heaviside function and ω_c is a cutoff energy. The quantities $\mu_{ij}^*(\omega_c)$ are the elements of the 3×3 Coulomb pseudopotential matrix. Finally, $N_j^\Delta(i\omega_m) = \Delta_j(i\omega_m) / \sqrt{\omega_m^2 + \Delta_j^2(i\omega_m)}$ and $N_j^Z(i\omega_m) = \omega_m / \sqrt{\omega_m^2 + \Delta_j^2(i\omega_m)}$.

The electron-boson coupling constants are defined as $\lambda_{ij}^{ph, sf} = 2 \int_0^{+\infty} d\Omega \frac{\alpha_{ij}^2 F^{ph, sf}(\Omega)}{\Omega}$. The solution of Eqs 4 and 5 requires a huge number of input parameters that can be taken from literature or fixed by suitable approximations (further details in the Supplementary Information). Then the critical temperature can be calculated, which turns out to be in agreement with the experimental one, once the “feedback” effect⁵⁶ of the electronic condensate on the antiferromagnetic spin fluctuations has been taken into account. The critical temperatures of the irradiated crystals are reproduced by setting a suitable non-zero interband scattering rate, as described above, in the *Results* section.

References

- Mazin, I. I., Singh, D. J., Johannes, M. D. & Du, M. H. Unconventional superconductivity with a sign reversal in the order parameter of LaFeAsO_{1-x}Fx. *Physical Review Letters* **101**, 057003, <https://doi.org/10.1103/physrevlett.101.057003> (2008).
- Chubukov, A. V., Efremov, D. V. & Eremin, I. Magnetism, superconductivity, and pairing symmetry in iron-based superconductors. *Physical Review B* **78**, 134512, <https://doi.org/10.1103/physrevb.78.134512> (2008).
- Kirshenbaum, K., Saha, S. R., Ziemak, S., Drye, T. & Paglione, J. Universal pair-breaking in transition-metal-substituted iron-pnictide superconductors. *Physical Review B* **86**, 140505(R), <https://doi.org/10.1103/physrevb.86.140505> (2012).
- Fernandes, R. M., Vavilov, M. G. & Chubukov, A. V. Enhancement of T_c by disorder in underdoped iron pnictide superconductors. *Physical Review B* **85**, 140512(R), <https://doi.org/10.1103/physrevb.85.140512> (2012).
- Onari, S., Kontani, H. & Sato, M. Structure of neutron-scattering peaks in both s₊₊-wave and s_±-wave states of an iron pnictide superconductor. *Physical Review B* **81**, 060504(R), <https://doi.org/10.1103/physrevb.81.060504> (2010).
- Efremov, D. V., Korshunov, M. M., Dolgov, O. V., Golubov, A. A. & Hirschfeld, P. J. Disorder-induced transition between s_± and s₊₊ states in two-band superconductors. *Physical Review B* **84**, 180512(R), <https://doi.org/10.1103/physrevb.84.180512> (2011).
- Wang, Y., Kreisel, A., Hirschfeld, P. J. & Mishra, V. Using controlled disorder to distinguish s_± and s₊₊ gap structure in Fe-based superconductors. *Physical Review B* **87**, 094504, <https://doi.org/10.1103/physrevb.87.094504> (2013).
- Schilling, M. B. *et al.* Tracing the s_± symmetry in iron pnictides by controlled disorder. *Physical Review B* **93**, 174515, <https://doi.org/10.1103/physrevb.93.174515> (2016).
- Cho, K. *et al.* Energy gap evolution across the superconductivity dome in single crystals of (Ba_{1-x}K_x)Fe₂As₂. *Science Advances* **2**, e1600807, <https://doi.org/10.1126/sciadv.1600807> (2016).
- Prozorov, R. *et al.* Effect of electron irradiation on superconductivity in single crystals of Ba(Fe_{1-x}Ru_x)₂As₂ (x = 0.24). *Journal of Applied Physics* **116**, 044302, <https://doi.org/10.1063/1.491032> (2014).
- Bang, Y. & Stewart, G. R. Superconducting properties of the s_±-wave state: Fe-based superconductors. *Journal of Physics: Condensed Matter* **29**, 123003, <https://doi.org/10.1088/1361-648x/aa564b> (2017).
- Karakozov, A. E. *et al.* Temperature dependence of the superfluid density as a probe for multiple gaps in Ba(Fe_{0.9}Co_{0.1})₂As₂: Manifestation of three weakly interacting condensates. *Physical Review B* **90**, 014506, <https://doi.org/10.1103/physrevb.90.014506> (2014).
- Prozorov, R. & Kogan, V. G. London penetration depth in iron-based superconductors. *Reports on Progress in Physics* **74**, 124505, <https://doi.org/10.1088/0034-4885/74/12/124505> (2011).
- Mishra, V. *et al.* Lifting of nodes by disorder in extended-s-state superconductors: Application to ferropnictides. *Physical Review B* **79**, 094512, <https://doi.org/10.1103/physrevb.79.094512> (2009).
- Karkin, A. E., Werner, J., Behr, G. & Goshchitskii, B. N. Neutron-irradiation effects in polycrystalline LaFeAsO_{0.9}F_{0.1} superconductors. *Physical Review B* **80**, 174512, <https://doi.org/10.1103/physrevb.80.174512> (2009).
- Tarantini, C. *et al.* Suppression of the critical temperature of superconducting NdFeAs(OF) single crystals by Kondo-like defect sites induced by α-particle irradiation. *Physical Review Letters* **104**, 087002, <https://doi.org/10.1103/physrevlett.104.087002> (2010).
- Cho, K. *et al.* Effects of electron irradiation on resistivity and London penetration depth of Ba_{1-x}K_xFe₂As₂ (x ≤ 0.34) iron-pnictide superconductor. *Physical Review B* **90**, 104514, <https://doi.org/10.1103/physrevb.90.104514> (2014).
- Mizukami, Y. *et al.* Disorder-induced topological change of the superconducting gap structure in iron pnictides. *Nature Communications* **5**, 5657, <https://doi.org/10.1038/ncomms5657> (2014).
- Tamegai, T. *et al.* Effects of particle irradiations on vortex states in iron-based superconductors. *Superconductor Science and Technology* **25**, 084008, <https://doi.org/10.1088/0953-2048/25/8/084008> (2012).
- Laviano, F. *et al.* Evidence of anisotropic vortex pinning by intrinsic and irradiation-induced defects in Ba(Fe,Co)₂As₂ studied by quantitative magneto-optical imaging. *Superconductor Science and Technology* **27**, 044014, <https://doi.org/10.1088/0953-2048/27/4/044014> (2014).
- Haberkorn, N. *et al.* Increment of the collective pinning energy in Na_{1-x}Ca_xFe₂As₂ single crystals with random point defects introduced by proton irradiation. *Superconductor Science and Technology* **27**, 095004, <https://doi.org/10.1088/0953-2048/27/9/095004> (2014).
- Ohtake, F., Taen, T., Pyon, S., Tamegai, T. & Okayasu, S. The effect of 320 MeV Au irradiation in K-doped Ba-122. *Physics Procedia* **58**, 122, <https://doi.org/10.1016/j.phpro.2014.09.046> (2014).
- Kihlstrom, K. J. *et al.* High-field critical current enhancement by irradiation induced correlated and random defects in (Ba_{0.6}K_{0.2})Fe₂As₂. *Applied Physics Letters* **103**, 202601, <https://doi.org/10.1063/1.4829524> (2013).
- Taen, T. *et al.* Effects of irradiation-particle energy on critical current density in Co-doped BaFe₂As₂. *Physica C: Superconductivity* **484**, 62, <https://doi.org/10.1016/j.physc.2012.02.040> (2013).
- Nakajima, Y. *et al.* Suppression of the critical temperature of superconducting Ba(Fe_{1-x}Co_x)₂As₂ by point defects from proton irradiation. *Physical Review B* **82**, 220504(R), <https://doi.org/10.1103/physrevb.82.220504> (2010).
- Taen, T. *et al.* Pair-breaking effects induced by 3-MeV proton irradiation in Ba_{1-x}K_xFe₂As₂. *Physical Review B* **88**, 224514, <https://doi.org/10.1103/physrevb.88.224514> (2013).
- Nakajima, Y. *et al.* Enhancement of critical current density in Co-doped BaFe₂As₂ with columnar defects introduced by heavy-ion irradiation. *Physical Review B* **80**, 012510, <https://doi.org/10.1103/physrevb.80.012510> (2009).
- Massee, F. *et al.* Imaging atomic-scale effects of high-energy ion irradiation on superconductivity and vortex pinning in Fe(Se,Te). *Science Advances* **1**, e1500033, <https://doi.org/10.1126/sciadv.1500033> (2015).
- Gozzelino, L., Gerbardo, R., Ghigo, G., Laviano, F. & Tamegai, T. Effects of 250 MeV Au-irradiation on the superconducting properties of Ba_{1-x}K_xFe₂As₂ single crystals. *MRS Advances* **1**, 3447, <https://doi.org/10.1557/adv.2016.428> (2016).
- Laviano, F. *et al.* Evidence of vortex curvature and anisotropic pinning in superconducting films by quantitative magneto-optics. *Physical Review B* **68**, 014507, <https://doi.org/10.1103/physrevb.68.014507> (2003).
- Allen, P. B. & Mitrović, B. Theory of superconducting T_c. *Solid State Physics* **37**, 1–92, [https://doi.org/10.1016/S0081-1947\(08\)60665-7](https://doi.org/10.1016/S0081-1947(08)60665-7) (1983).
- Efremov, D., Golubov, A. & Dolgov, O. Manifestations of impurity-induced s_± s₊₊ transition: multiband model for dynamical response functions. *New Journal of Physics* **15**, 013002, <https://doi.org/10.1088/1367-2630/15/1/013002> (2013).
- Efremov, D., Korshunov, M., Dolgov, O., Golubov, A. A. & Hirschfeld, P. Disorder-induced transition between s_± and s₊₊ states in two-band superconductors. *Physical Review B* **84**, 180512, <https://doi.org/10.1103/PhysRevB.84.180512> (2011).
- Korshunov, M. M., Togushova, Y. N. & Dolgov, O. V. Impurities in multiband superconductors. *Physics-Uspekhi* **59**, 1211, <https://doi.org/10.3367/UFNe.2016.07.037863> (2016).
- Mazin, I. & Schmalian, J. Pairing symmetry and pairing state in ferropnictides: Theoretical overview. *Physica C: Superconductivity* **469**, 614–627, <https://doi.org/10.1016/j.physc.2009.03.019> (2009).
- Boeri, L., Calandra, M., Mazin, I. I., Dolgov, O. V. & Mauri, F. Effects of magnetism and doping on the electron-phonon coupling in BaFe₂As₂. *Physical Review B* **82**, 020506, <https://doi.org/10.1103/PhysRevB.82.020506> (2010).
- Charnukha, A. *et al.* Eliashberg approach to infrared anomalies induced by the superconducting state of Ba_{0.68}K_{0.32}Fe₂As₂ single crystals. *Physical Review B* **84**, 174511, <https://doi.org/10.1103/PhysRevB.84.174511> (2011).
- Ghigo, G., Ummarino, G., Gozzelino, L. & Tamegai, T. Penetration depth of Ba_{1-x}K_xFe₂As₂ single crystals explained within a multiband Eliashberg s_± approach. *Physical Review B* **96**, 014501, <https://doi.org/10.1103/PhysRevB.96.014501> (2017).

39. Ghigo, G., Gerbaldo, R., Gozzelino, L., Laviano, F. & Tamegai, T. Penetration depth and quasiparticle conductivity of Co- and K-doped BaFe₂As₂ crystals, investigated by a microwave coplanar resonator technique. *IEEE Transactions on Applied Superconductivity* **26**, 1, <https://doi.org/10.1109/tasc.2016.2529419> (2016).
40. Ding, H. *et al.* Observation of fermi-surface-dependent nodeless superconducting gaps in (Ba_{0.6}K_{0.4})Fe₂As₂. *EPL (Europhysics Letters)* **83**, 47001, <https://doi.org/10.1209/0295-5075/83/47001> (2008).
41. Eliashberg, G. Interactions between electrons and lattice vibrations in a superconductor. *Sov. Phys. JETP* **11**, 696–702 (1960).
42. Chubukov, A., Pines, D., Schmalian, J., KH, B. & Ketterson, J. A spin fluctuation model for d-wave superconductivity. In *Superconductivity: Volume 1: Conventional and Unconventional Superconductors Volume 2: Novel Superconductors*, 1349–1413 (Springer, 2008).
43. Manske, D., Eremin, I., Bennemann, K. & Ketterson, J. Electronic theory for superconductivity in high-T_c cuprates and Sr₂RuO₄. In *Superconductivity: Volume 1: Conventional and Unconventional Superconductors Volume 2: Novel Superconductors*, 1415–1515 (Springer, 2008).
44. Umbarino, G. Iron-based layered compounds: the effect of negative interband coupling. *Journal of superconductivity and novel magnetism* **22**, 603–607, <https://doi.org/10.1007/s10948-009-0459-8> (2009).
45. Popovich, P. *et al.* Specific heat measurements of Ba_{0.68}K_{0.32}Fe₂As₂ single crystals: evidence for a multiband strong-coupling superconducting state. *Physical review letters* **105**, 027003, <https://doi.org/10.1103/PhysRevLett.105.027003> (2010).
46. Dolgov, O. & Golubov, A. A. Strong electron-phonon interaction in multiband superconductors. *Physical Review B* **77**, 214526, <https://doi.org/10.1103/PhysRevB.77.214526> (2008).
47. Hwang, J. Electron-boson spectral density function of correlated multiband systems obtained from optical data: (Ba_{0.6}K_{0.4})Fe₂As₂ and LiFeAs. *Journal of Physics: Condensed Matter* **28**, 125702, <https://doi.org/10.1088/0953-8984/28/12/125702> (2016).
48. Ziegler, J. F., Ziegler, M. & Biersack, J. SRIM – the stopping and range of ions in matter (2010). *Nuclear Instruments and Methods in Physics Research Section B: Beam Interactions with Materials and Atoms* **268**, 1818–1823, <https://doi.org/10.1016/j.nimb.2010.02.091> (2010).
49. Sato, T. *et al.* Particle and Heavy Ion Transport code System, PHITS, version 2.52. *Journal of Nuclear Science and Technology* **50**, 913–923, <https://doi.org/10.1080/00223131.2013.814553> (2013).
50. Ghigo, G., Laviano, F., Gerbaldo, R. & Gozzelino, L. Tuning the response of YBCO microwave resonators by heavy-ion patterned micro-channels. *Superconductor Science and Technology* **25**, 115007, <https://doi.org/10.1088/0953-2048/25/11/115007> (2012).
51. Hardy, W. N., Bonn, D. A., Morgan, D. C., Liang, R. & Zhang, K. Precision measurements of the temperature dependence of λ in YBa₂Cu₃O_{6.95}: Strong evidence for nodes in the gap function. *Physical Review Letters* **70**, 3999–4002, <https://doi.org/10.1103/physrevlett.70.3999> (1993).
52. Vendik, I. Phenomenological model of the microwave surface impedance of high-T_c superconducting films. *Superconductor Science and Technology* **13**, 974–982, <https://doi.org/10.1088/0953-2048/13/7/312> (2000).
53. Umbarino, G. A. Multiband s± Eliashberg theory and temperature-dependent spin-resonance energy in iron pnictide superconductors. *Physical Review B* **83**, 092508, <https://doi.org/10.1103/physrevb.83.092508> (2011).
54. Umbarino, G. A., Tortello, M., Daghero, D. & Gonnelli, R. S. Three-band s± Eliashberg theory and the superconducting gaps of iron pnictides. *Physical Review B* **80**, 172503, <https://doi.org/10.1103/physrevb.80.172503> (2009).
55. Umbarino, G. A., Daghero, D., Tortello, M. & Gonnelli, R. S. Predictions of multiband s± strong-coupling Eliashberg theory compared to experimental data in iron pnictides. *Journal of Superconductivity and Novel Magnetism* **24**, 247–253, <https://doi.org/10.1007/s10948-010-1006-3> (2010).
56. Umbarino, G. A. Effects of magnetic impurities on two-band superconductor. *Journal of Superconductivity and Novel Magnetism* **20**, 639–642, <https://doi.org/10.1007/s10948-007-0259-y> (2007).

Acknowledgements

This work was supported by MIUR-PRIN2012 Project No. 2012X3YFZ2. The irradiations were performed in the framework of the INFN-Politecnico di Torino M.E.S.H. Research Agreement. G.A.U. acknowledges support from the MEPhI Academic Excellence Project (Contract No. 02.a03.21.0005).

Author Contributions

G.G. conceived the experiment and made the microwave characterizations, G.A.U. made the Eliashberg calculations, and T.T. fabricated the samples. Irradiations were performed by G.G., L.G., R.G. and F.L., and D.T. contributed to data analysis. Damage simulations were done by L.G. and D.T. All the authors discussed the results and reviewed the manuscript.

Additional Information

Supplementary information accompanies this paper at <https://doi.org/10.1038/s41598-017-13303-5>.

Competing Interests: The authors declare that they have no competing interests.

Publisher's note: Springer Nature remains neutral with regard to jurisdictional claims in published maps and institutional affiliations.



Open Access This article is licensed under a Creative Commons Attribution 4.0 International License, which permits use, sharing, adaptation, distribution and reproduction in any medium or format, as long as you give appropriate credit to the original author(s) and the source, provide a link to the Creative Commons license, and indicate if changes were made. The images or other third party material in this article are included in the article's Creative Commons license, unless indicated otherwise in a credit line to the material. If material is not included in the article's Creative Commons license and your intended use is not permitted by statutory regulation or exceeds the permitted use, you will need to obtain permission directly from the copyright holder. To view a copy of this license, visit <http://creativecommons.org/licenses/by/4.0/>.

© The Author(s) 2017